The 2009 IEEE/RSJ International Conference on
Intelligent Robots and Systems
October 11-15, 2009 St. Louis, USA

Configurations and Mathematical Models of Parallel Link Mechanisms Using Multi Drive Linear Motors

Takashi Harada, *Member, RSJ* and Motoya Nagase

***Abstract*—In this paper, parallel link mechanisms for multi drive linear motors (MDLMs) are proposed. The multi drive is a control method for linear motors in which a number of moving parts are individually driven on one stator part. Various configurations of parallel link mechanisms which were constructed for MDLMs are proposed. These mechanisms offer a wide range of motion in addition to the existing characteristics that parallel mechanisms provide, namely, rigid mechanisms, high precision, and high speed. Moreover, they are suitable for force control because of their low friction direct drive actuators. In this paper, the kinematic and dynamic characteristics of 2-DOF (*xy*) and 3-DOF (*xy*θ) planar parallel link mechanisms are investigated. A singularity analysis and internal force control method for a 3-DOF with 4 redundant moving parts is derived. The condition of dynamic decoupling and the constant inertia design of a 2-DOF with 2 moving parts and a 3-DOF with 4 moving parts are derived. The effectiveness of these analyses is then confirmed by numerical simulation. Based on this analysis, a prototype of the 3-DOF with 4 moving parts is designed and developed.**

I. Introduction

A robotic system with parallel link mechanisms (PLMs) has mechanical characteristics such as rigidity of the mechanism and precise positioning [1]-[3]. These characteristics enable them to stably perform contact tasks with sensitive force, e.g. mold grindings and rehabilitation robotics. On the other hand, mechanical interference and the singularity of the mechanism restrict the robot's movable range [4]. PLMs have therefore been conventionally applied not to general-purpose industrial robots, but to special-purpose machines [5]-[6].

In order to expand this limited application of PLMs, new parallel link mechanisms with multi drive linear motors (MDLMs) are proposed. The multi drive is a control method for linear motors in which a number of moving parts are individually driven on one stator part. In this paper, we propose various configurations of PLMs that were constructed for MDLMs. These PLMs expand the robot's movable range while retaining the advantageous rigid mechanism and precise positioning that PLMs offer. Moreover, the proposed PLMs are suitable for force control, because linear motors are directory driven without friction full gearings. In this paper, we investigate the kinematics and dynamic characteristics of 2-DOF (*xy*) with 2 moving parts (2D2M), and 3-DOF (*xy*θ) with 3 non-redundant moving parts- (3D3M) and 4 redundant moving parts- (3D4M) planar parallel link mechanisms. The redundancy of the PLMs is not used only for singularity avoidance as sought by conventional research, but is also used for forward kinematics computation [7] and calibration of the mechanism [8][9], which have been standing problems with conventional PLMs.

Manuscript received March 1, 2009. This work was supported in part by the Electro-Mechanic Technology Advancing Foundation, Japan.

T. Harada is with the Department of Mechanical Engineering, Faculty of Science and Engineering, Kinki University, Osaka, Japan. (corresponding author to provide phone: +81-6-6721-2332 ; fax: +81-6-6727-2024; e-mail: harada@mech.kindai.ac.jp).

M. Nagase is with the Graduate School of Kinki University, Osaka, Japan.

II. Configurations of Link Mechanism

A. Multi Drive Linear Motor

A ball screw driven by a rotational motor, as shown in Fig.1 (a), is generally used as a linear actuator in conventional PLMs. A single driving part moves in a straight line on a linear stator; we will refer to this below as a single drive. A single drive disturbs the space in which movement takes place, and restricts the general-purpose application of PLMs. Moreover, it is difficult in principal for the load of the tip to be transmitted to the actuator, which in turn renders the ball screw drive incapable of force control.

To cope with these problems, multi drive linear motors (MDLMs), as shown in Fig.1 (b), were employed in our research. MDLMs offer a way to arrange more than one moving part on one stator of a linear motor, with each moving part individually controlled and driven.

Various configurations of parallel link mechanisms that were constructed for MDLMs are proposed. These mechanisms offer a wide range of motion, in addition to the existing characteristics that parallel mechanisms offer,

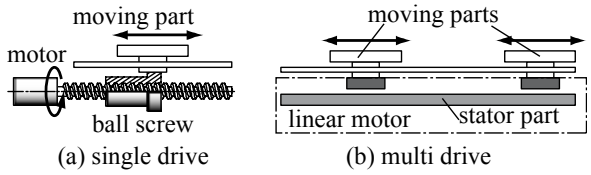

Fig. 1. Single and multi drive linear motors

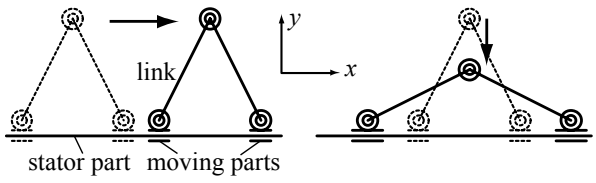

Fig. 2. 2D2M parallel link mechanism

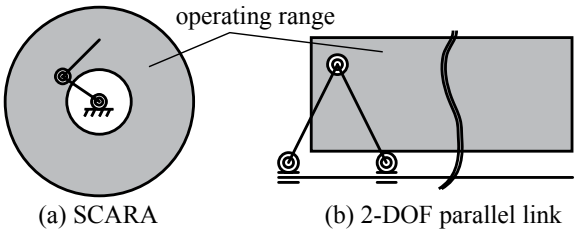

Fig. 3. Operating range of the SCARA and the 2D2M parallel link

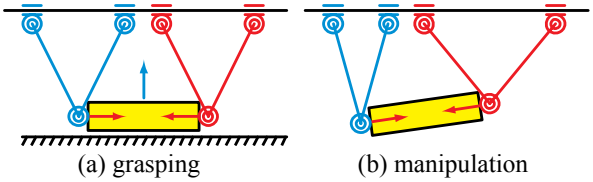

Fig. 4. Grasping and manipulation by 2x2D2M parallel links

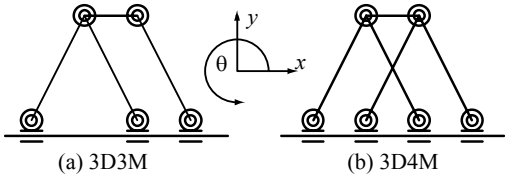

Fig. 5. 3-DOF planar parallel link mechanisms

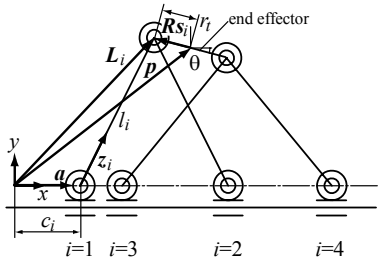

Fig. 6. Kinematic model of the 3-DOF planar parallel link mechanisms

namely rigid mechanisms, high precision and high speed.

In this paper, the kinematics and dynamic characteristics of 2-DOF (xy) with 2 moving parts on one stator (2D2M), and 3-DOF ($xy\theta$) with 3 non-redundant moving parts- (3D3M) and with 4 redundant moving part- (3D4M) planar parallel link mechanisms are investigated. It is possible to expand the range of motion of PLMs to three dimensions by using more than two stators.

B. Configuration of 2-DOF Planar Mechanism

The configuration of a 2D2M planar PLM is shown in Fig. 2. The 2D2M PLM has mechanical characteristics such that the mechanical compliance on the horizontal (xy) plane is higher than that of the vertical (z) direction. It is suitable for part-fitting tasks in a vertical direction, such as SCARA (Selective Compliance Assembly Robot Arm). In addition, the PLM has a wide range of motion in the x direction, as shown in Fig. 3.

Moreover, it is possible to arrange the heavy moving parts on the base so that the weight of the link mechanisms is reduced, allowing for faster motion and greater accuracy than in a SCARA. Figure 4 shows another application using a pair of 2D2M PLMs. This system has 4 moving parts on a single linear stator, which can perform the tasks of grasping, conveying and manipulation.

C. Configuration of 3-DOF Planar Mechanism

The configuration of a 3-DOF ($xy\theta$) planar PLM with 3 non-redundant moving parts (3D3M) and a 3-DOF ($xy\theta$) planar PLM with 4 redundant moving parts (4D4M), are shown in Figs. 5(a) and (b). The 3D4M PLM with 4 redundant moving parts is the centerpiece of our research. Its redundancy is used not only for singularity avoidance, but also for forward kinematics computation and calibration of the mechanism. We are planning to apply the PLM to a table mechanism of 5 axis machine tools.

III. Kinematics of the Parallel Link Mechanism

A. Kinematics of 3-DOF Parallel Link Mechanisms

On the basis of the general kinematics formulation of parallel link mechanisms [10] [11], a kinematics equation for the proposed 3-DOF parallel link mechanism was derived. In turn, the parallel link mechanism of the particular configuration of our research can also be analyzed by the general method of kinematics.

The kinematic relationships of the 3D4M PLM, as shown in Fig. 6, are expressed as follows:

$$\begin{aligned} &\boldsymbol{p} + \boldsymbol{R}\boldsymbol{s}_i = \boldsymbol{L}_i = c_i\boldsymbol{a} + l_i\boldsymbol{z}_i \\ &\boldsymbol{p} = [x, y]^T, \boldsymbol{a} = [1,0]^T \\ &\boldsymbol{s}_1 = \boldsymbol{s}_2 = [-r_t, 0]^T, \boldsymbol{s}_3 = \boldsymbol{s}_4 = [r_t, 0]^T \\ &\boldsymbol{R} = \begin{bmatrix} \cos\theta & -\sin\theta \\ \sin\theta & \cos\theta \end{bmatrix} \end{aligned} \tag{1}$$

where c_i (i = 1,..,4) is the control variable of the ith actuator, i.e., the position of the ith moving part of the multi drive linear motor. The length of the ith rod (link) is expressed as l_i. The distance from the central point to the ith pair of the end effecter is expressed as r_t. Other symbols are indicated as in Fig. 6. Equation (1) expresses the relationship between the positions of the moving parts c_i (i=1,..,4) and the positions $\boldsymbol{p}$ and orientation θ of the end effecter. By solving (1) as c_i, an inverse kinematics equation is derived as follows:

$$c_i = \boldsymbol{L}_i^T\boldsymbol{a} \pm \sqrt{(\boldsymbol{L}_i^T\boldsymbol{a})^2 - (\boldsymbol{L}_i^T\boldsymbol{L}_i)^2 + l_i^2} \tag{2}$$

For the 1st and 3rd link, the plus-minus sign in (3) is given as positive, and for 2nd and 4th link is given as negative. The

unit direction vector of the *i*th link is given as:

$$\boldsymbol{z}_i = (\boldsymbol{L}_i - c_i\boldsymbol{a})/l_i \tag{3}$$

By applying derivatives to both sides of (1), the derivative relation of the 3D4M PLM is derived as follows:

$$\begin{aligned}
&\boldsymbol{J}_{e43}\Delta\boldsymbol{p}_3 = \boldsymbol{J}_{c4}\Delta\boldsymbol{c}_4 \\
&\Delta\boldsymbol{p}_3 = [\Delta x, \Delta y, \Delta\theta]^T, \Delta\boldsymbol{c}_4 = [\Delta c_1, ..., \Delta c_4]^T \\
&\boldsymbol{J}_{e43} = \left[\begin{array}{c|c} \boldsymbol{z}_1^T & \boldsymbol{z}_1^T(\boldsymbol{R}_\theta\boldsymbol{R}\boldsymbol{s}_1) \\ \vdots & \vdots \\ \boldsymbol{z}_4^T & \boldsymbol{z}_4^T(\boldsymbol{R}_\theta\boldsymbol{R}\boldsymbol{s}_4) \end{array}\right], \boldsymbol{J}_{c4} = \begin{bmatrix} \boldsymbol{z}_1^T\boldsymbol{a} & \cdots & 0 \\ \vdots & \ddots & \vdots \\ 0 & \cdots & \boldsymbol{z}_4^T\boldsymbol{a} \end{bmatrix} \\
&\boldsymbol{R}_\theta = \begin{bmatrix} 0 & -1 \\ 1 & 0 \end{bmatrix}
\end{aligned} \tag{4}$$

where $\boldsymbol{J}_{e44}$ and $\boldsymbol{J}_{c4}$ are Jacobian matrices of the system. Kinematic characteristics such as singular point and static force can be analyzed by using (4).

The kinematic equation of the 3D3M PLM is derived by removing the redundant part from (1)-(4) as follows:

$$\begin{aligned}
&\boldsymbol{J}_{e33}\Delta\boldsymbol{p}_3 = \boldsymbol{J}_{c3}\Delta\boldsymbol{c}_3 \\
&\Delta\boldsymbol{p}_3 = [\Delta x, \Delta y, \Delta\theta]^T, \Delta\boldsymbol{c}_3 = [\Delta c_1, \Delta c_2, \Delta c_3]^T
\end{aligned} \tag{5}$$

B. Kinematics of the 2-DOF Parallel Link Mechanisms

The kinematic equation of the 2D2M PLM shown in Fig. 2 is derived as $\boldsymbol{s}_i$=0 in (1)-(3). The differential equation of the 2D2M PLM is given as:

$$\begin{aligned}
&\boldsymbol{J}_{e22}\Delta\boldsymbol{p}_2 = \boldsymbol{J}_{c2}\Delta\boldsymbol{c}_2 \\
&\Delta\boldsymbol{p}_2 = [\Delta x, \Delta y]^T, \Delta\boldsymbol{c}_2 = [\Delta c_1, \Delta c_2]^T \\
&\boldsymbol{J}_{e22} = \begin{bmatrix} \boldsymbol{z}_1^T \\ \boldsymbol{z}_2^T \end{bmatrix}, \boldsymbol{J}_{c2} = \begin{bmatrix} \boldsymbol{z}_1^T\boldsymbol{a} & 0 \\ 0 & \boldsymbol{z}_2^T\boldsymbol{a} \end{bmatrix}
\end{aligned} \tag{6}$$

C. Singularity Analysis of the 3-DOF PLM

It is well known that parallel link mechanisms have two kinds of singularities [12][13]. When PLM arrives at a position and orientation such that the Jacobian matrix $\boldsymbol{J}_{cm}$ in (4)-(6) is singular, the output of the actuators does not transfer to the link mechanism. These situations are referred to as 1st kind of singularity. When the PLM arrives at a position and orientation such that the Jacobian matrix $\boldsymbol{J}_{en}$ in (4)-(6) is singular, the output of the end effecter does not transfer to the link mechanism. These situations are referred to as 2nd kind of singularity. Variables *m* and *n* express the number of actuators and the degree of freedom of the end effecter, respectively.

When each element of $\boldsymbol{J}_{cm}$ equals zero, the proposed PLM becomes the 1st kind of singularity. The condition of the 1st kind of singularity is expressed as follows:

$$\boldsymbol{z}_i^T\boldsymbol{a} = 0 \tag{7}$$

Equation (7) implies that if the unit direction vector $\boldsymbol{a}$ of the actuator and the unit direction vector $\boldsymbol{z}_i$ of each link are orthogonal, the PLM becomes one of 1st class singular points.

The 2nd kind of singularity differs, depending on the configuration of the PLM. Here, the singular points of the 3D3M PLM are derived. The condition of the 2nd kind of singularity is given as the determinant of the Jacobian matrix in (5), which equals zero as follows:

$$\det(\boldsymbol{J}_{e33}) = 0 \tag{8}$$

Using symbolic mathematics software, equation (8) is solved. The following 4 types of singular points exist in the 3D3M PLM.

$$\text{Type 1: } \theta = \sin^{-1}(y/r_t) \tag{9}$$

$$\text{Type 2: } \theta = \sin^{-1}((\pm l_i + y)/r_t) \tag{10}$$

$$\text{Type 3: } \theta = \pm\cos^{-1}(\sqrt{((l_i - r_t)^2 - y^2)/(l_i - r_t)^2}) \tag{11}$$

$$\text{Type 4: } \theta = \pm\cos^{-1}(\sqrt{((l_i + r_t)^2 - y^2)/(l_i + r_t)^2}) \tag{12}$$

Next, the singularity avoidance of the 3D4M PLM is shown through the definition of manipulability [14]. The derivative kinematics of the PLM is transformed as:

$$\Delta\boldsymbol{c}_m = \boldsymbol{J}_{cm}^{-1}\boldsymbol{J}_{enm}\Delta\boldsymbol{p}_n = \boldsymbol{J}_{cenm}\Delta\boldsymbol{p}_n \tag{13}$$

The manipulability of the PLM is defined as follows:

$$w = \sqrt{\det(\boldsymbol{J}_{cenm}^T\boldsymbol{J}_{cenm})} \tag{14}$$

Numerical calculations of the manipulability of the 3D3M PLM and the 3D4M PLM in correspondence with the rotation angle of the end effecter, are shown in Figs. 7(a)

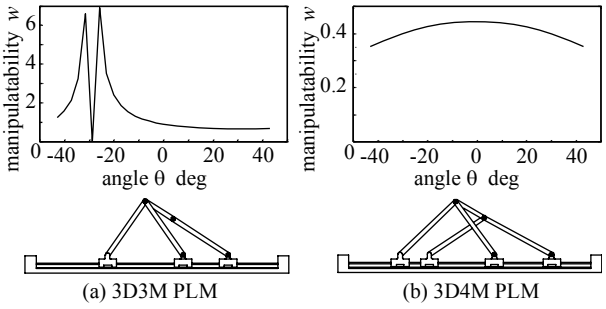

Fig. 7. Singularity analysis of the parallel link mechanisms

and (b). The ratio of each link length l_i and the length of the end effecter $2r_t$ is given as 2:1.

The 3D3M non-redundant PLM becomes the 4th type of singular point given in (12) when the angle of the end effecter equals 28.7 degrees. Around this angle value, there is little manipulability, as shown in Fig.7 (a). On the other hand, the singular point is avoided by the redundant 3D4M PLM, as shown in Fig.7 (b). This confirms that the redundancy of the 3D4M PLM greatly increases homogeneous manipulability.

IV. Static Force Analysis of the PLM

A. Static Force Analysis for the non-redundant PLM

Conventional static force analysis only derives the relationship between the generative force/torque of actuators and the ***external forces*** of the end effecter based on the principle of virtual force. Here, we expand this static force analysis in order to also calculate ***internal forces*** such as the constraint forces at the joints and the axial forces of the links.

First, the formula for static force is derived when the degree of freedom of the end effecter (n) and the actuators (m) is equivalent. For the sake of convenience, the external forces of the end effecter $\boldsymbol{f}_e$ and the generative forces of the actuators $\boldsymbol{f}_c$ are expressed by vector forms as follows:

$$\begin{aligned} \boldsymbol{f}_e &= [f_x, f_y]^T (n=2), [f_x, f_y, \tau_\theta]^T (n=3) \\ \boldsymbol{f}_c &= [f_{c1}, \ldots, f_{cm}]^T \end{aligned} \tag{15}$$

The relationship between $\boldsymbol{f}_e$ and $\boldsymbol{f}_c$ is derived by the principle of virtual forces as:

$$\begin{aligned} \boldsymbol{f}_e &= \boldsymbol{J}_{cenm}{}^T \boldsymbol{f}_c \\ \boldsymbol{f}_c &= (\boldsymbol{J}_{cenm}{}^T)^{-1} \boldsymbol{f}_e \end{aligned} \tag{16}$$

As shown in Fig. 8, f_{ni} and f_{li} are defined as quantities of the constraint force at the ith joint and axial force of the ith link, respectively. The values f_{ni} and f_{li} represent the internal forces

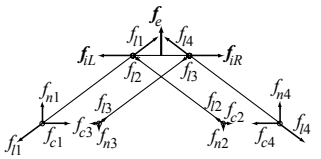

Fig. 8. Relations of forces

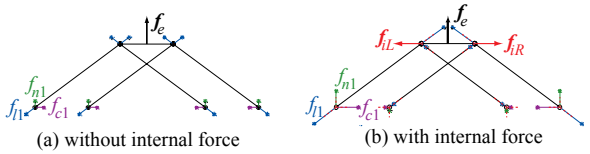

Fig. 9. Numerical simulation about static forces

of the PLM. The unit direction vector $\boldsymbol{n}$ along the constraint force f_{ni} is orthogonal to the unit direction vector $\boldsymbol{a}$ along the actuator force f_{ci}. The equilibrium of forces at the ith joint is given as:

$$f_{ci}\boldsymbol{a} + f_{ni}\boldsymbol{n} + f_{li}\boldsymbol{z}_i = \boldsymbol{0} \tag{17}$$

By applying the inner product to (17) with each vector $\boldsymbol{a}$ and $\boldsymbol{n}$, with the condition that vectors $\boldsymbol{a}$ and $\boldsymbol{n}$ are mutually orthogonal, the following formulas are derived:

$$\begin{aligned} f_{ci} + (\boldsymbol{z}_i{}^T \boldsymbol{a}) f_{li} &= 0 \\ f_{ni} + (\boldsymbol{z}_i{}^T \boldsymbol{n}) f_{li} &= 0 \end{aligned} \tag{18}$$

The constraint force f_{ni} and the axial force f_{li} of each link are combined as vector form $\boldsymbol{f}_n$ and $\boldsymbol{f}_l$ as follows:

$$\begin{aligned} \boldsymbol{f}_c &= -diag(\boldsymbol{z}_1{}^T \boldsymbol{a}, \ldots, \boldsymbol{z}_m{}^T \boldsymbol{a}) \cdot \boldsymbol{f}_l = -\boldsymbol{J}_{cm} \boldsymbol{f}_l \\ \boldsymbol{f}_n &= -diag(\boldsymbol{z}_1{}^T \boldsymbol{n}, \ldots, \boldsymbol{z}_m{}^T \boldsymbol{n}) \cdot \boldsymbol{f}_l = -\boldsymbol{J}_{nm} \boldsymbol{f}_l \end{aligned} \tag{19}$$

From (15) to (19), the internal forces $\boldsymbol{f}_n$ and $\boldsymbol{f}_l$ are given by the following equations:

$$\begin{aligned} \boldsymbol{f}_n &= (\boldsymbol{J}_{nm} \boldsymbol{J}_{cm}{}^{-1}) \boldsymbol{f}_c \\ \boldsymbol{f}_l &= -\boldsymbol{J}_{cm}{}^{-1} \boldsymbol{f}_c \end{aligned} \tag{20}$$

B. Static Force Analysis for the redundant PLM

In this section, the static forces for the redundant 3D4M PLM, as shown in Fig. 5 (b), are derived. Instead of the inverse matrix of (16), a generalized inverse matrix is applied to the calculation of the static force equation.

$$\boldsymbol{f}_c = (\boldsymbol{J}_{cenm}{}^T)^+ \boldsymbol{f}_e + (\boldsymbol{I} - (\boldsymbol{J}_{cenm}{}^T)^+ \boldsymbol{J}_{cenm}{}^T) \boldsymbol{k} \tag{21}$$

where $^+$ implies the pseudo inverse of a matrix, and $\boldsymbol{k}$ is a 1×4 arbitrary vector. In the case of the 3D4M PLM, the left side of (21) has 4 degrees of freedom. On the right side of (21), the 1st term has 3 degrees of freedom, which means the 2nd term will have 1 degree of freedom.

The null space projection matrix $\boldsymbol{I} - (\boldsymbol{J}_{cenm}{}^T)^+ \boldsymbol{J}_{cenm}{}^T$ is 4×4, but its rank is just one. Therefore, the dimension of the 2nd term on the right side of (21) is reduced as:

$$\begin{aligned} (\boldsymbol{I} - (\boldsymbol{J}_{cenm}{}^T)^+ \boldsymbol{J}_{cenm}{}^T) \boldsymbol{k} &= \boldsymbol{J}_{cenm}{}^T \boldsymbol{J}_i{}^{-1} \boldsymbol{f}_i \\ \boldsymbol{J}_i &= -\begin{bmatrix} \boldsymbol{z}_1 & \boldsymbol{z}_2 & \boldsymbol{0} & \boldsymbol{0} \\ \boldsymbol{0} & \boldsymbol{0} & \boldsymbol{z}_3 & \boldsymbol{z}_4 \end{bmatrix} \\ \boldsymbol{f}_i &= \begin{bmatrix} \boldsymbol{f}_{iR} \\ \boldsymbol{f}_{iL} \end{bmatrix} = f_i [\cos\theta, \sin\theta, -\cos\theta, -\sin\theta]^T \end{aligned} \tag{22}$$

The dimension was reduced to one by the independent

variable f_i in (22). In its physical sense, f_i corresponds to the quantity of internal force acting on the end effecter plate.

In (22), $\boldsymbol{f}_{iL}$ and $\boldsymbol{f}_{iR}$ are the internal forces which act upon the left and right ends of the end plate, respectively, as shown in Fig. 8. For purposes of convenience, they are combined together as the vector $\boldsymbol{f}_i$. The direction of internal forces $\boldsymbol{f}_{iL}$ and $\boldsymbol{f}_{iR}$ coincides with the direction of the end plate, whose angle is defined by the rotation angle θ of the end effecter. The values $\boldsymbol{f}_{iL}$ and $\boldsymbol{f}_{iR}$ have the same quantity f_i, but have opposite directions, as shown in Fig. 8. The one dimensional internal force that acts along the end plate is explicitly controlled by (22).

Finally, from (21) and (22), the generative forces of the actuators $\boldsymbol{f}_c$ are calculated from the external force of the end effecter $\boldsymbol{f}_e$ and the internal force of the end plate $\boldsymbol{f}_i$ as:

$$\boldsymbol{f}_c = (\boldsymbol{J}_{cenm}{}^T)^+ \boldsymbol{f}_e + \boldsymbol{J}_{cenm}{}^T \boldsymbol{J}_i{}^{-1} \boldsymbol{f}_i \tag{23}$$

The internal force of the end plate exerts tensile or compressive stress on the end plate, which helps to diminish joint backlash and increase mechanical rigidity [15].

C. Numerical Simulation of the Static Force Analysis

Numerical simulation software of the static force analysis for the 3D4M PLM, as shown in Fig. 5(b), was developed. The external force $\boldsymbol{f}_e$, the internal force $\boldsymbol{f}_i$, the generative force of the actuator $\boldsymbol{f}_c$, the constraint force $\boldsymbol{f}_n$ and the tensile force of the link $\boldsymbol{f}_L$ were calculated for an arbitrary position and orientation of the PLM. Schematic views of these forces superimposed on the link mechanism are shown in Fig. 8. Examples of static force simulations for the 3D4M PLM are shown in Figs. 9 (a) and (b).

Unit external force $\boldsymbol{f}_e$ is acting at the central position of the end plate. Fig. 9 (a) shows the case in which the internal force of the end plate $\boldsymbol{f}_i$ is zero. Representations of the generative force of the actuator $\boldsymbol{f}_c$, the constraint force $\boldsymbol{f}_n$ and the tensile force of the link $\boldsymbol{f}_L$ are superimposed on the link mechanism as a solid line with the symbol * at the tip of the vector. Fig. 9 (b) shows the case in which the unit internal force of the end plate $\boldsymbol{f}_i$ was applied. In Fig. 9(b), the internal force $\boldsymbol{f}_i$ and additional forces caused by the $\boldsymbol{f}_i$ at each joint are shown by broken lines. Representations of the generative force of the actuator $\boldsymbol{f}_c$, the constraint force $\boldsymbol{f}_n$ and the tensile force of the link $\boldsymbol{f}_L$ are also superimposed on the link mechanism as a solid line with the symbol * at the tip of the vector. These forces include elements of the internal force $\boldsymbol{f}_i$, from (23).

The situation in Fig. 9 (b) expresses how compressive force was exerted upon the end plate. This situation also expresses how two 2D2M PLMs grasp an object with compressive force, as shown in Fig. 4.

V. Dynamics of the Parallel Link Mechanism

A. Equation of Motion of the 2D2M PLM

An equation of motion for the 2D2M PLM was derived, and is shown in Fig.2. In order to focus on the dynamic characteristics of the link mechanisms, the mass of the actuator was excluded from this equation of motion.

The position of the end effecter $\boldsymbol{p}=[x, y]^T$ and of the generative forces at the end effecter $\boldsymbol{f}_e=[f_x, f_y]^T$ are considered as generalized positions and generalized forces, respectively. In this formulation, gravity was assumed to be affected in the negative direction of the y-axis. The equation of motion was derived by applying Lagrange's equation.

In particular, if the length, mass and moment of inertia of each link is designed with the same value, the equation of motion of the PLM becomes a simple formula, as follows:

$$\begin{bmatrix} f_x \\ f_y \end{bmatrix} = \begin{bmatrix} m_{xx} & 0 \\ 0 & m_{yy}(y) \end{bmatrix} \ddot{\boldsymbol{p}} + \begin{bmatrix} 0 \\ h_y(y, \dot{y}) \end{bmatrix} + \begin{bmatrix} 0 \\ g_y \end{bmatrix} \tag{24}$$

where m_{xx} and m_{yy} denote the generalized inertia of the PLM. The value m_{xx} is a constant and m_{yy} is a function of $\boldsymbol{y}$. Non-diagonal elements of the inertia matrix are zero. Elements h_y and g_y express Coriolis and centrifugal forces, and the gravitational force of the y direction, respectively. Elements of Coriolis, centrifugal and gravitational forces of the x direction are zero.

Equation (24) reveals that the dynamics of the $\boldsymbol{x}$ direction of the 2D2M PLM has both ***decoupled and constant inertia*** characteristics. The dynamics in the y direction are also decoupled in the x direction. Moreover, the inertia m_{yy} and the Coriolis and centrifugal force h_y are functions of only y. The constant of gravitational force affects only the y direction.

B. Equation of Motion of the 3D4M PLM

An equation of motion for the 3D4M PLM was derived, as shown in Fig.5 (b).

The positions and orientation of the end effecter $\boldsymbol{p}=[x, y, \theta]^T$ and the generative forces/torque at the end effecter $\boldsymbol{f}_e=[f_x, f_y, \tau_\theta]^T$ are considered as generalized positions and generalized forces, respectively. In this formulation, gravity was assumed to be affected by the negative direction of the y-axis. The equation of motion was derived by applying Lagrange's equation.

In particular, if the length, mass and moment of inertia of each link is designed with the same value, the equation of motion of the PLM becomes a simple formula, as follows:

$$\begin{bmatrix} f_x \\ f_y \\ \tau_\theta \end{bmatrix} = \begin{bmatrix} m_{xx} & 0 & 0 \\ 0 & m_{yy}(\boldsymbol{q}) & m_{y\theta}(\boldsymbol{q}) \\ 0 & m_{y\theta}(\boldsymbol{q}) & m_{\theta\theta}(\boldsymbol{q}) \end{bmatrix} \ddot{\boldsymbol{p}} + \begin{bmatrix} 0 \\ h_y(\boldsymbol{q}, \dot{\boldsymbol{q}}) \\ h_\theta(\boldsymbol{q}, \dot{\boldsymbol{q}}) \end{bmatrix} + \begin{bmatrix} 0 \\ g_y \\ 0 \end{bmatrix} \tag{25}$$

$$\boldsymbol{q} = [y, \theta]^T$$

Equation (25) shows that the dynamics of the $\boldsymbol{x}$ direction of the 3D4M PLM has both ***decoupled and constant inertia*** characteristics. The dynamics of the y and θ directions are also decoupled in the x direction. The constant of

gravitational force affects only the *y* direction.

As we showed in (24) and (25), if the mechanical parameters of each link are designed with the same value, the equation of motion becomes a simple formula.

C. Numerical Simulation of the Dynamics

Numerical simulations of the dynamics of the 3D4M PLM were tested. One example is shown in Fig.10. In the simulation, the length, mass and moment of inertia of each link were given as 0.14m, 0.064kg and 1.97E-4 kgm^2, respectively. The length, mass and moment of inertia of the end plate were given as 0.10m, 0.375kg and 8.54E-4 kgm^2, respectively. The initial positions and orientation were set as $\boldsymbol{p}_0$=[0.0m, 0.10m, -20.0deg]^T. A constant force f_x=0.1N was applied to the end effecter. The time responses of positions *x* and *y*. are shown in Fig.10 (a). No conflict was observed between the *x* and *y* directions. The configurations of the PLM at intervals of 0.1 sec are shown in Fig.10 (b). The PLM generated a constant motion of acceleration in the *x* direction while maintaining its initial configuration.

VI. Experimental System of the 3D4M PLM

An experimental system of the 3D4M PLM was developed. The 3D CAD model and prototype design of the experimental system are shown in Figs.11 (a) and (b). A front view while the orientation of the end plate is being changed is shown in Fig. 12. The four moving parts of a linear shaft motor with a rated force of 2.3N were individually driven and controlled on a stator shaft with a length of 950mm. A linear encoder

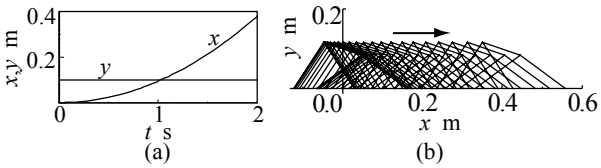

Fig. 10. Numerical simulation of dynamics

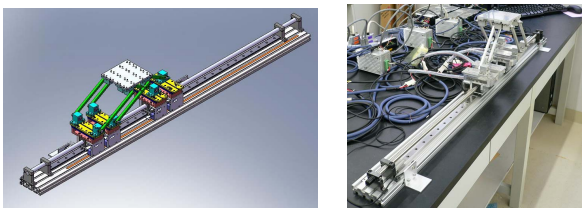

(a) 3D CAD model (b) prototype of the PLM

Fig. 11. 3D CAD model and prototype of the experimental system

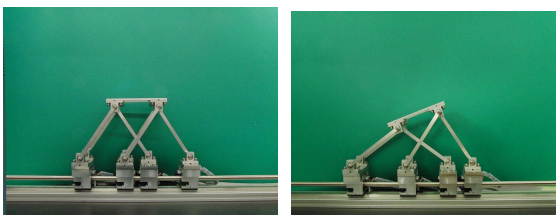

Fig. 12. Front view of the experimental system

with a positional resolution of 1μm was installed on each driving part of the linear motor. The length of each link and end plate was designed as 0.14 m and 0.10 m, respectively. The mass and moment of inertia of each link were designed with the same value in order to realize the decoupled and constant inertia dynamics shown in the previous section.

VII. Conclusion

New parallel link mechanisms for multi drive linear motors were proposed. These expand their range of motion, while retaining the advantages of a rigid mechanism and precise positioning. A prototype of a 3-DOF planar PLM with 4 redundant moving parts was designed and developed by applying the results of the present study of static force and dynamics analysis, as follows:

1) Static force analysis was expanded to calculate internal forces such as the axial forces of links. This was useful for the mechanical design of the PLM.
2) If the length, mass and moment of inertia of each link were designed with the same value, the equation of motion of the PLM showed both decoupled and constant inertia characteristics in the *x* direction.

References

[1] D. Stewart, "A platform with six degrees of freedom," *Proc. Instn. Mech. Engrs.*, vol.180, part I, no.15, pp. 371-386, 1966.

[2] J. P. Merlet, "Parallel Robotics," Kluwer Academic Pub, 2000.

[3] J. Wang and X. J. Liu, "Parallel Robotics," Nova Science Pub Inc., 2008.

[4] J. P. Merlet, "Singular configurations of parallel manipulators and grassmann geometry," *Int. J. of Robotics Research*, vol.8, no.5, pp. 45-56, 1989.

[5] M. Weck, "Parallel kinematic machine tools-current state and future potentials," *Annals of the CIRP*, vol.51, no.2, pp. 671-683, 2002.

[6] T. Oiwa, "New coordinate measuring machine featuring a parallel mechanism," *Int. J. JSPE*, vol.31, no.3, pp. 232-233, 1997.

[7] J. P. Merlet, "Direct kinematics of planar parallel manipulators," *IEEE Trans. Robotics Automat.* vol.9, no.6, pp. 842-845, 1993.

[8] H. Zhuang and L. Liu, "Determination of number of independent parameters for the self-calibration of parallel-link mechanisms," *in Proc ASME*, MED-vol.8, pp. 699-703, 1998.

[9] Y. J. Chiu and M. H. Perg, "Self-calibration of a general hexapod manipulator using cylindrical constraints," *Int. J. Macine Tools & Manufct.*, vol. 43, pp. 1051-1066, 2003.

[10] T. Arai, "Development of a parallel link manipulator," *in Proc. 5th ICAR*, vol. 1, pp. 839-844, 1991.

[11] T. Arai, "Analysis and synthesis of a parallel link manipulator based on its statics," *JRSJ*, vol. 10, no. 4, pp. 526-533, 1992.

[12] C. Gosselin and J. Angeles, "Singularity analysis of closed-loop kinematic chains," *IEEE Trans. Robotics and Automation,* vol. 6, no.3, pp. 281-290, 1990.

[13] T. Kokkins and R. Stroughton, "Optimal parallel actuation linkage for 3 dof elbow manipulators," *The 1988 ASME Des, Tech. Conf*, vol. DE-15-3, pp. 465-472, 1988.

[14] T. Yoshikawa, "Manipulability of robotic mechanisms," *in Preprints Int. Symp. Robot Res.*, pp. 439-446, 1985.

[15] M. A. Adli, K. Nagai, K. Miyataka and H. Hanafusa, "Internal force analysis and its applications in parallel manipulators," *in Proc 1990 Jpn-USA Symp Flex Autom.*, vol. 1, pp. 69-72, 1990.

[16] T. Yoshikawa and K. Nagai, "Manipulating and grasping forces in manipulation by multi fingered robot hands," *IEEE Trans. Robotics and Automation*, vol. 7, no.1, pp. 67-77, 1991.